Sustained delivery of thermostabilized chABC enhances axonal sprouting and functional recovery after spinal cord injury

Hyunjung Lee[a], Robert J. McKeon[b], and Ravi V. Bellamkonda[a,1]

[a]Wallace H. Coulter Department of Biomedical Engineering, Georgia Institute of Technology and Emory University, Atlanta, GA 30332 and [b]Department of Cell Biology, Emory University School of Medicine, Atlanta, GA 30322

Edited by Robert Langer, Massachusetts Institute of Technology, Cambridge, MA, and approved September 16, 2009 (received for review May 15, 2009)

Chondroitin sulfate proteoglycans (CSPGs) are a major class of axon growth inhibitors that are up-regulated after spinal cord injury (SCI) and contribute to regenerative failure. Chondroitinase ABC (chABC) digests glycosaminoglycan chains on CSPGs and can thereby overcome CSPG-mediated inhibition. But chABC loses its enzymatic activity rapidly at 37 °C, necessitating the use of repeated injections or local infusions for a period of days to weeks. These infusion systems are invasive, infection-prone, and clinically problematic. To overcome this limitation, we have thermostabilized chABC and developed a system for its sustained local delivery in vivo, obviating the need for chronically implanted catheters and pumps. Thermostabilized chABC remained active at 37 °C in vitro for up to 4 weeks. CSPG levels remained low in vivo up to 6 weeks post-SCI when thermostabilized chABC was delivered by a hydrogel-microtube scaffold system. Axonal growth and functional recovery following the sustained local release of thermostabilized chABC versus a single treatment of unstabilized chABC demonstrated significant differences in CSPG digestion. Animals treated with thermostabilized chABC in combination with sustained neurotrophin-3 delivery showed significant improvement in locomotor function and enhanced growth of cholera toxin B subunit–positive sensory axons and sprouting of serotonergic fibers. Therefore, improving chABC thermostability facilitates minimally invasive, sustained, local delivery of chABC that is potentially effective in overcoming CSPG-mediated regenerative failure. Combination therapy with thermostabilized chABC with neurotrophic factors enhances axonal regrowth, sprouting, and functional recovery after SCI.

chondroitin sulfate | glial scar | glycosaminoglycans | hydrogel

After injury to the central nervous system, lesioned axons fail to regrow (1). Although exploring the cellular and molecular mechanisms of regenerative failure after spinal cord injury (SCI) is an active area of research, no effective clinical therapy exists. A major impediment to regeneration is the development of astroglial scarring at the site of injury. After injury to the central nervous system (CNS), a cascade of cellular and molecular responses culminates in the formation of a dense astroglial scar at the lesion site (2, 3). Macrophages, microglia, oligodendrocyte precursors, meningeal cells, and astrocytes migrate into the lesion and produce inhibitory molecules, such as myelin-associated glycoprotein and chondroitin sulfate proteoglycans (CSPGs). The final "product" is a tightly interwoven glial scar surrounding the lesion site composed primarily of CSPGs and reactive astrocytes.

chABC, a bacterial enzyme that digests the chondroitin sulfate glycosaminoglycans (CS-GAGs) of CSPGs, promotes axonal sprouting and functional recovery in various animal models (4). chABC promotes sprouting in both intact and injured spinal cords (5) and in the visual cortex (6, 7) by digesting CSPGs present in an astroglial scar and enhancing plasticity by digesting CSPGs in perineuronal nets (PNNs).

Several factors limit the use of chABC in vivo. chABC is thermally sensitive and almost all of its enzymatic activity is lost within 3–5 days at 37 °C (8). Generally, CSPGs are up-regulated and accumulate in the lesion site for at least 2 weeks after the initial injury (9). Therefore, for chABC to degrade CSPG-associated glycosaminoglycans (GAGs), a "fresh" supply would be needed at least every 2 weeks. Currently this is achieved via intrathecal injection, with the infusion frequency varying from days to weeks and the duration of therapy ranging from 2 to 6 weeks (10–13). But diffusion of chABC into deep regions of the cord is limited when it is delivered intrathecally, due to overflow beyond the intrathecal space and attendant dilution, necessitating compensatory high-dose infusions (2–1,000 U/mL). Consequently, there is a compelling need to develop clinically viable methods for the spatially and temporally controlled delivery of chABC, preferably in a manner that confines it to the lesion site.

Here we report a novel method to thermostabilize chABC using the sugar trehalose and describe a hydrogel-microtube based delivery system that facilitates sustained local delivery of chABC in vivo. Our data demonstrate that the enzymatic activity of trehalose-stabilized chABC is maintained for up to 4 weeks at 37 °C in vitro. Thermostabilized chABC (TS-chABC) retains its ability to digest CSPGs in vivo 2 weeks postinjury, and CS-GAG levels remain significantly depleted at the lesion site for at least 6 weeks post-SCI. Enhanced axonal sprouting and functional recovery is observed when TS-chABC is delivered either alone or in combination with neurotrophin-3 (NT-3).

Results

Trehalose Significantly Enhances chABC Thermal Stability and Prolongs Enzyme Activity. The enzymatic activity of unstabilized and trehalose-stabilized chABC was evaluated by investigating the enzyme's ability to digest the CSPG decorin, followed by SDS-PAGE analysis. Decorin has a simple molecular structure consisting of one chondroitin or dermatan sulfate GAG chain on its core protein. Intact decorin migrated as a higher–molecular weight (MW) broad smear on an SDS-PAGE gel (Fig. 1*A*, lane 1) and as a tighter lower-MW band after digestion with chABC (≈40–45 kDa; Fig. 1*A*, lane 4). chABC alone migrated between 97 kDa and 116 kDa (Fig. 1*A*, lane 2). chABC preincubated for 24 h at 37 °C retained its ability to degrade (Fig. 1*A*, lane 5) decorin, but lost its ability to completely degrade decorin GAGs after 1 week of preincubation at 37 °C (Fig. 1*A*, lane 6).

In contrast, following incubation with 1 M trehalose at 37 °C for 1 week, TS-chABC retained its ability to degrade decorin (Fig. 1*A*, lane 8). Different concentrations of trehalose were evaluated; concentrations above 500 mM successfully preserved chABC activity for 2 weeks of incubation at 37 °C.

Author contributions: H.L., R.J.M., and R.V.B. designed research; H.L. performed research; H.L. analyzed data; and H.L. and R.V.B. wrote the paper.

The authors declare no conflict of interest.

This article is a PNAS Direct Submission.

[1]To whom correspondence should be addressed. E-mail: ravi@gatech.edu

This article contains supporting information online at www.pnas.org/cgi/content/full/0905437106/DCSupplemental.

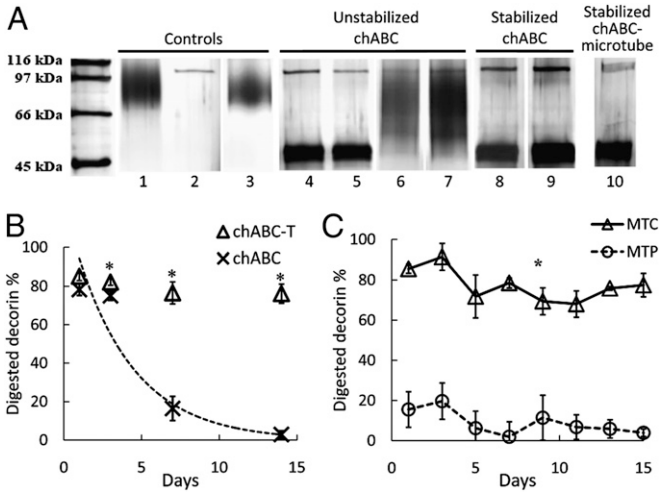

Fig. 1. Enhanced thermal stability of chABC with trehalose, and sustained chABC release with lipid microtubes. (*A*) SDS-PAGE assay of enzymatic activity of chABC. Controls: lane 1, intact decorin; lane 2, fresh chABC; lane 3, fresh penicillinase + decorin. Unstabilized chABC: lane 4, fresh chABC + decorin; lane 5, 1 day preincubated chABC + decorin; lane 6, 1 week preincubated chABC + decorin; lane 7, 4 weeks preincubated chABC + decorin. Trehalose-stabilized chABC: lane 8, 1 week; lane 9, 4 weeks preincubated chABC/T + decorin. Stabilized chABC-microtube: lane 10, chABC released from microtube + decorin. (*B*) Kinetic analysis of chABC deactivation by DMMB assay. The *x*-axis represents days; the *y*-axis represents percentage of digested decorin. Asterisks denote a significant difference from chABC in 1× PBS ($P < .05$). Data are expressed as mean ± SEM. The dotted line represents the calculated deactivation curve of chABC in 1× PBS. (*C*) Enzymatic activity of postreleased chABC (Δ) and penicillinase (○) with trehalose/microtubes. All data points are significantly different ($P < .05$; mean ± SEM).

After 1 M trehalose and chABC were coincubated for 4 weeks at 37 °C, the mxture was added to decorin. Lane 9 in Fig. 1*A* shows that the trehalose-stabilized chABC digested decorin. In comparison, chABC lost its activity after 4 weeks of incubation in PBS at 37 °C without trehalose (Fig. 1*A*, lane 7). Decorin incubated with fresh chABC (Fig. 1*A*, lanes 4) and intact decorin (incubated for 4 h at 37 °C; Fig. 1*A*, lane 1) were included as controls at the same time. Penicillinase was used as a control enzyme, and when decorin was incubated with penicillinase (Fig. 1*A*, lane 3) at 37 °C, no decorin digestion was observed.

Temperature Stabilization of chABC by Trehalose Is Due to Conformational Stability. Temporal deactivation profiles of chABC enzymatic activity with and without trehalose were determined via a dimethylmethylene blue (DMMB) assay (Fig. 1*B*). At every time point except day -1, there was a significant difference between the control and trehalose-treated samples. chABC activity was maintained up to day -15 with trehalose. In comparison, without trehalose, chABC lost its enzymatic activity after day -3 and was completely inactive by day -5. Based on this deactivation study, a kinetic deactivation constant, k_d, was evaluated by assuming a 2-state transition between the native state (N) to the unfolded state (D),

$$\mathrm{N}\rightarrow\mathrm{D};\ \mathrm{dN/dt} = -k_d\mathrm{N};\ n = \mathrm{N}_0\exp(-k_d t)$$

where N_0 represents initial N and the first-order kinetics was adapted (the dotted line in Fig. 1*B*). The deactivation rate constant of chABC was computed to be 0.27 (day^{-1}; $R^2 = 0.98$).

To investigate whether the increased thermostability of chABC in the presence of trehalose is due to conformational stabilization, conformational changes in chABC as a function of temperature with and without trehalose were quantified by circular dichroism (CD) [supporting information (SI) Fig. S1]. Details of the CD method and analysis (14) are given in SI Text. The midpoint transition temperature (T_m), the enthalpy of denaturation (ΔH_m), and the entropy of denaturation (ΔS_m) of chABC were 64.2 °C, 171 $kJ{\cdot}mol^{-1}$, and 506 $J\ K^{-1}mol^{-1}$ in the 1 M trehalose solution and 56.2 °C, 176 $kJ{\cdot}mol^{-1}$, and 533 $J\ K^{-1}\ mol^{-1}$ in the buffer solution. The increment in the midpoint of transition, ΔT_m, is 8 °C, indicating that chABC's conformation is thermally more stable in the presence of 1 M trehalose.

Table 1. Experimental design with notation

Notation	Components	*n*
MTC*†	Agarose gel scaffold embedded with microtubes loaded with chABC and trehalose	8
MT*	Agarose gel scaffold embedded with microtubes loaded with trehalose	6
STC*	Single injection of chABC with trehalose	8
SC*	Single injection of chABC	6
MTP*†	Agarose gel scaffold embedded with microtubes loaded with penicillinase and trehalose	6
STP*	Single injection of penicillinase with trehalose	6
noT*	Injury and no treatment	6
Sham*,†	Conducted the same procedure except injury with other groups	4
MTN†	Agarose gel scaffold embedded with microtubes loaded with NT-3	7
MTCN†	Agarose gel scaffold embedded with microtubes loaded with chABC/trehalose and NT-3	8
GC†	Agarose gel mixed with chABC/trehalose	6

M, lipid microtubes; S, single injection; T, trehalose; C, chABC; P, penicillinase.
*Conditions for 2-week study.
†Conditions for 45-day study.

Microtube-Encapsulated chABC Is Biologically Active for 2 Weeks. To verify that self-assembled, hollow lipid microtubes (0.5 μm × 40 μm) can be loaded with chABC without compromising its activity, the ability of chABC released from fresh microtubes (without preincubation at 37 °C) to digest decorin was tested by SDS-PAGE (Fig. 1*A*, lane 10). As indicated by the digested decorin band, microtube loading did not negatively impact chABC activity. Next, the activity of chABC and penicillinase released from microtubes was plotted as a function of time (Fig. 1*C*), and their relative enzymatic activity was measured by a DMMB assay (15, 16). The finding of 100% of digested decorin on the *y*-axis connotes complete digestion of decorin. When combined with trehalose, chABC released from microtubes retained its enzymatic activity up to 15 days in vitro at 37 °C. The combination of penicillinase and trehalose did not digest decorin.

Sustained Delivery of Encapsulated chABC Digests CSPGs Effectively in Vivo. CS-56 and 3B3 immunostaining was used to investigate chABC's activity in vivo when delivered via the lipid microtube-hydrogel system (Fig. S2). The 3B3 antibody recognizes unsaturated, C6-sulfated GAG stubs (17) and is a marker for successful CSPG digestion by chABC. The CS-56 antibody was used to identify intact, undigested CSPG. GFAP immunoreactivity (GFAP-IR) was used to identify reactive astrocytes and, in combination with either 3B3 or CS-56, to define the lesion boundary. Two weeks after hemisection SCI, tissue sections from the microtube-trehalose-chABC (MTC)-treated animals (see Table 1 for notation of groups) showed significantly high 3B3-IR near the lesion site (Fig. 2*E*), while CS-56–IR at adjacent tissue sections was lower (Fig. 2*D*). CS-56–IR was high at the lesion boundary but was significantly reduced overall. In the no-treatment (NoT) group, the opposite IR was observed, with strong CS-56–IR and no 3B3-IR (Fig. 2*A* and *B*). Similar patterns were observed in the other control groups. Fluorescent pixel intensity was used to quantify 3B3-IR and

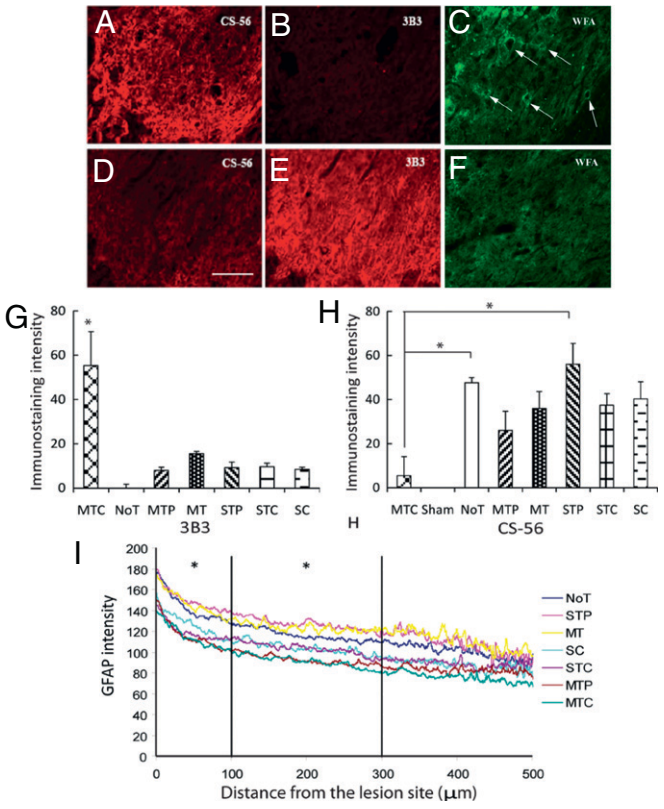

Fig. 2. Immunohistologic analysis of CSPG digestion in vivo (*A–F*) and quantitative image analysis of 3B3, CS-56, and GFAP (*G–I*). CS-56-IR for CSPGs (*A* and D), 3B3-IR for digested CSPGs (*B* and *E*), and WFA staining for PNNs (*C* and *F*). The intensity of CS-56–IR and WFA is inversely proportional to 3B3-IR. Images were taken immediately next to the lesion boundary of NoT (*A–C*) and microtube-trehalose-chABC treated (*D–F*) animals. Arrows in (*C*) indicate WFA-PNNs. (Scale bar: 100 μm.) (*G*) 3B3-IR quantitative analysis. *, $P < .05$ denotes a significant increase of 3B3-IR in MTC treatment compared to all other treatments. (*H*) CS-56-IR quantitative analysis. *, $P < .05$ denotes a significant decrease of CS-56–IR in MTC compared with NoT and STP treatments. No significant differences were observed among other treatments. (*I*) Line profile analysis of GFAP-IR. GFAP-IR is decreased as a function of distance; it is significantly lower in the MTC group compared with the control groups NoT, STP, and MT in the 0–100 μm and 100–300 μm intervals (*, $P < .05$). Data are mean ± SEM.

CS-56–IR (Fig. 2*G* and *H*) using ImagePro software. 3B3-IR was significantly higher in the MTC group compared with all other groups (Fig. 2*G*; $P < .05$). The average CS-56–IR was significantly lower in the MTC group in than the other groups, and there was a statistically significant difference in CS-56–IR between the MTC and NoT/STP groups (Fig. 2*H*; $P < .05$).

The integrity of PNNs in the vicinity of the lesion site was examined using *Wisteria floribunda* agglutinin (WFA) cytochemistry on the same tissue sections that were stained with 3B3. WFA is a lectin specific for N-acetylgalactosamine and visualizes net-like structures of PNNs. Positive WFA staining represents intact PNNs, and reduced WFA staining represents digested PNNs because of chABC-mediated digestion of CSPGs. Intact PNNs were observed near the lesion site in the STC, NoT (Fig. 2*C*), and other conditions; significantly less WFA staining was observed in the MTC condition (Fig. 2*F*). Immunostaining of WFA, 3B3, and CS-56 showed the presence of WFA-PNNs when CS-56–IR intensity was strong and 3B3-IR was weak or absent. In the MTC, the 3B3-positive region in which CSPGs were degraded by chABC had no WFA-PNNs and low CS-56—IR, indicating that sustained delivery of chABC resulted in significantly diminished PNNs close to the lesion boundary, increasing the permissivity for axonal sprouting.

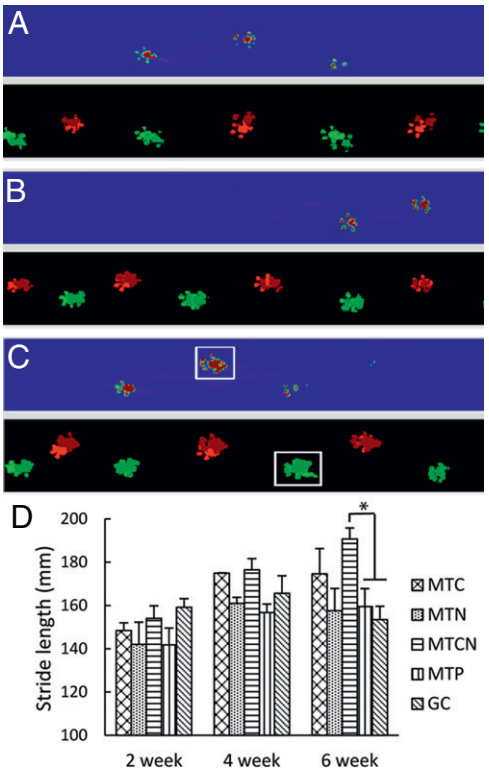

Fig. 3. CatWalk raw data in false color mode. (*A*) Sham, (*B*) MTCN, and (*C*) MTP animals on the walkway at 6 weeks. All groups show a normal step sequence. The white boxes in (*C*) represent an abnormal hind paw print. (*D*) Stride length analysis for locomotion functional recovery. Data are mean ± SEM. An asterisk denotes statistical significance between MTCN and MTP, and between MTCN and GC ($P < .05$).

GFAP-positive astrocytes were used to define the scar area and the boundaries of the lesion. Fluorescent pixel intensity was quantified using a custom image analysis program developed in MATLAB that measures intensity from the lesion interface into the cord radially (18). The intensity of GFAP-IR decreased from the lesion site into the cord, and the number of reactive astrocytes also decreased and correlated positively with CS-56–IR intensity. The analyzed intensity was divided into 3 spatial bins located 0–100, 100–300, and 300–500 μm away from the lesion interface. GFAP-IR was significantly lower in the MTC group compared with the NoT, STP, and MT groups in the 0–100 μm and 100–300 μm bins (Fig. 2*I*; $P < .05$). These data confirm that our sustained delivery system dd not negatively impact the astrogliotic response.

Sustained Delivery of chABC and NT-3 Improves Locomotor Function. In a separate cohort of animals, functional recovery was assessed 45 days post-SCI using the CatWalk and thermal plantar tests. A significant improvement in locomotor function in MTCN animals was observed 6 weeks post-SCI (Fig. 3) but not earlier, and no improvement with the thermal pain threshold test was seen in any of the groups throughout the testing period. At day 7 and day 14, all animal groups exhibited abnormal walking pattern, slow crossing, and abnormal paw prints, reflecting SCI-mediated dysfunction. Four weeks postsurgery, most animals recovered a normal step sequence and demonstrated improved crossing time.

At 6 weeks post-SCI, a significant difference in the stride length among the treatment groups was seen (Fig. 3). The average stride length (mean ± SEM) was 183.6 ± 6.91 mm for MTCN, 172.89 ± 20.8 mm for MTC, 157 ± 18.25 mm for MTN, 152.91 ± 13.13 mm for GC, and 154.07 ± 10.11 mm for MTP. Significant differences

were observed between MTCN and GC ($P = .019$) and between MTCN and MTP ($P = .035$).

At 6 weeks, the MTCN, MTC, and MTN animals had more normal footprints (Fig. 3*B*) compared with the MTP animals (white boxes in Fig. 3*C*). The number of abnormal hind paw prints per 3 step cycles was quantified; the averages were 0.7 ± 0.3 for MTCN, 1.7 ± 0.6 for MTC, 1.8 ± 0.5 for MTN, 2.1 ± 1.3 for GC, and 3.3 ± 1.3 for MTP. The mean number of abnormal prints of the single-treated animals, MTC and MTN, was less than that of animals treated by GC and MTP; on average, the MTCN animals had even fewer abnormal foot prints. While these are strong trends, the differences are not statistically significant. Similarly, no statistically significant differences in base support or hind paw withdrawal latency were observed among the treated groups.

Sustained Delivery of chABC and NT-3 Promotes Sprouting. When cholera toxin B subunit (CTB) was injected into the sciatic nerve, retracted CTB-labeled fibers in the glial scar area were observed, along with a few fibers that approached the lesion site in the MTP and GC groups (Fig. S3 *A* and *C*). But in the MTC, MTN, and MTCN groups, more CTB-labeled fibers crossed the glial scar, approached the lesion boundary (Fig. S3*B*), and grew around cavities along the lesion interface (Fig. S3*D*). Significantly more fibers crossed 0 and 0.5 mm rostral to the caudal edge of the lesion in the MTCN group compared with the GC and MTP groups ($P =$ .03 and .045; $P = .049$ and .045; Fig. 4*A*). In the MTC, MTN, and MTCN groups, a few fibers were observed at 1 mm rostral to the lesion; however, no fibers entered the lesion cavity.

In the MTC, MTN, and MTCN groups, more serotonergic 5-HT IR fibers were observed in the gray matter, predominantly in the ventral horn and lamina X, and more fibers were found rostral versus caudal to the lesion (Fig. 4*B*). Quantification confirmed that MTCN treatment resulted in significant sprouting of serotonergic fibers caudal to the lesion compared with all other treatments ($P =$ .008 for MTC, $P = .024$ for MTN, $P = .001$ for GC, and $P = .001$ for MTP) and rostral to the lesion compared with MTN ($P = .015$), GC ($P = .002$), and MTP ($P = .001$) treatments (Fig. 4*E*).

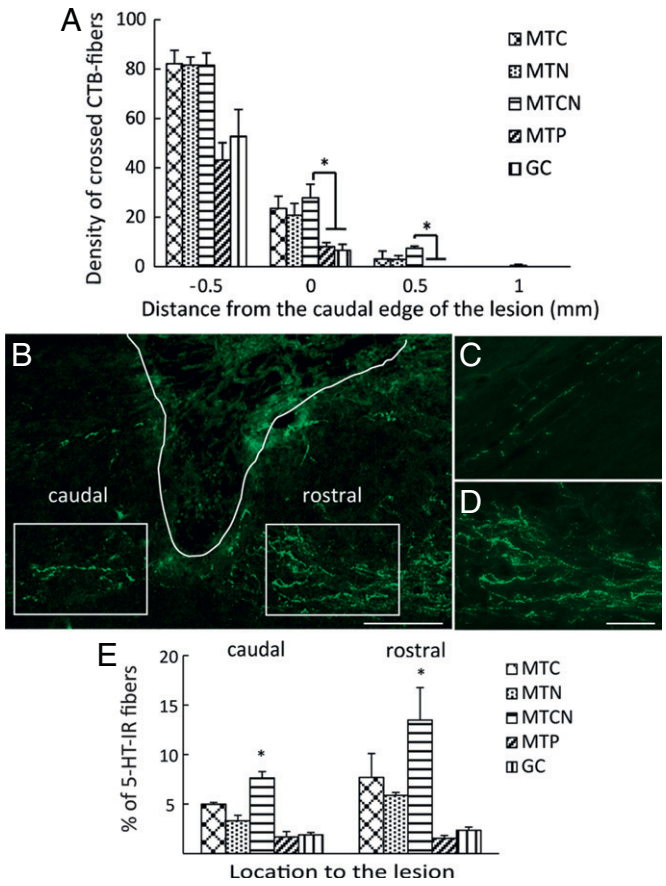

Fig. 4. Quantification of CTB+ axon growth and immunohistological analysis of 5-HT–IR fiber. (*A*) The *y*-axis represents the density of crossed axons at the distance to the lesion interface, and the *x*-axis represents distance to the lesion (mm). Asterisks denote a significant difference compared with MTCN ($P < .05$). (*B*) Micrograph of 5-HT at 4× magnification in the MTCN-treated tissue. The boxed areas denote regions selected for quantification, and the solid white line represents the lesion interface. (Scale bar: 500 μm.) (*C* and *D*) Serotonergic innervations rostral to the lesion in the MTP (*C*) and MTCN (*D*). (Scale bar: 100 μm.) (*E*) Quantification demonstrated that caudal to the lesion, MTCN showed significantly ($P < .05$) increased 5-HT–IR compared with all other treatments, and that rostral to the lesion, MTCN showed significantly ($P < .05$) increased 5-HT–IR compared with all other treatments except for MTC. Data are mean ± SEM.

Discussion

Thermal instability of chABC represents a significant impediment to overcoming CSPG-mediated inhibition after SCI because it constrains sustained drug delivery approaches, necessitating indwelling catheter–mediated delivery. Here we demonstrate that trehalose stabilizes chABC activity at 37 °C. TS-chABC delivered by a lipid microtube-hydrogel scaffold system was enzymatically active in situ for at least 2 weeks in vitro, and when delivered in vivo, resulted in low levels of CSPG for 6 weeks. Locomotor behavior improved with combination chABC–NT3 delivery and correlated with axonal sprouting at the lesion site. This study demonstrates that a single treatment of TS-chABC via the hydrogel-microtube delivery system provides an effective alternative to the chronically implanted invasive pumps typically used to deliver chABC in vivo.

The molecular mechanism of trehalose-mediated thermostabilization is poorly understood (19). There are several hypotheses outlining the mechanisms of protein stabilization by trehalose, including water replacement (20), preferential hydration (21), vitrification of solutions (22), and the influence of trehalose on the water–tetrahedral hydrogen bond network (23). Previous studies have shown that surface tension of trehalose solutions increases linearly with increasing trehalose concentration (24), and there is a strong correlation between surface tension and increased T_m (25). The dynamic fluctuation of polar side chains at the solvent–protein interface is reduced in the presence of trehalose (19). The increased surface tension or the limited exposure of hydrophobic groups to the water molecules leads to preferential hydration, resulting in stabilization of the tertiary structure of protein (21). In this study, the ΔT_m of chABC with trehalose (8 °C) is similar to the effects of trehalose on other enzymes, such as RNase A (5.5 °C) and lysozyme (8.4 °C) (25), where increased conformational thermostabilization positively influences enzymatic activity. Thus, trehalose's ability to thermally stabilize chABC is consistent with its effects on other enzymes.

The time course of peak deposition of CSPG at the lesion site is dependent on the type of CSPG (9). Neuron-glial antigen 2 is an important CSPG expressed after SCI, with expression peaking between 1 and 2 weeks after injury. Expression levels of other CSPGs, such as neurocan, brevican, and versican, also are elevated after SCI, peak at 2 weeks, and are maintained for 4 weeks or more. We chose the 14-day post-SCI time point to analyze the effectiveness of TS-chABC because CSPG expression levels are highest at ≈18 days post-SCI (26).

Our laboratory has previously reported the use of lipid microtubes for the delivery of proteins (27), DNA (28), and neurotrophic factors in vivo (29). Relative to other polyester-based delivery systems, lipid microtubes have the advantage of no protein exposure to heat or organic solvents. Lipid microtubes are injectable either by themselves or embedded in thermoreversible hydrogels (18). Here microtube-gel scaffold provides sustained delivery of

TS-chABC over a 2-week period, with the microtubes enabling slow release and the hydrogel localizing the tubes to the lesion site. We have developed a mathematical model (27) to predict the release profile of compounds with a range of MWs, such as myoglobin (17.8 kDa), albumin (66.4 kDa), and thyroglobulin (660 kDa). The model suggests that an initial burst release of protein from day 1 to day 3 is followed by a slow release, leading to a cumulative percentage of released agent of 80%–100% by day 14. Because the MW of chABC (120 kDa) is within the protein MW range measured previously, most of the chABC loaded into microtubes is likely released by day 14.

To compare the effect of sustained delivery versus single administration, a dose of TS-chABC (STC) equal to the total amount of chABC loaded into microtubes over 14 days was injected at the lesion site. This single injection had no effect, as reflected by a lack of 3B3 staining. Thus, sustained release of chABC is critical, because chABC diffuses away after the injection and CSPG production continues over time. 3B3-IR was significantly higher in the MTC group compared with all of the other groups. It is interesting that in the STC group, small bright spots of 3B3-IR were observed around the lesion site (gray matter), possibly because the chABC digested some CSPGs before being washed out. It is difficult to ascertain the activity of released chABC over time in vivo. Once chABC is released from the delivery system, its activity can be assumed to be similar to that of fresh, unstabilized chABC, because the trehalose–chABC ratio becomes diluted. But because the microtubes serve as reservoirs for TS-chABC, this is akin to an injection of fresh chABC every 2 weeks. CS-56 staining at 6 weeks (Fig. S4) showed little persistent CS-56 expression compared with that in untreated controls. This suggests that TS-chABC digestion was effective early, at the peak of CSPG production, and its turnover was slow. PNNs also were degraded following microtube-mediated release of chABC. In comparison, a single injection of chABC was not sufficient to break down PNNs. In the MTC group, PNNs were not observed near the lesion site but were present ≈1 mm away from the site, suggesting that TS-chABC activity was localized to the region in the immediate vicinity of the lesion. chABC is a relatively large molecule, and its diffusion through neural tissue is limited. Compared with intrathecal delivery of chABC via a catheter, chABC delivered via our delivery system diffuses deeper into the tissue (up to 1 mm), because intrathecal delivery affects a larger region, diluting the chABC, whereas our delivery system enables local delivery into the tissue. As CSPG deposition tapers off exponentially from the lesion border, the local delivery of chABC is relevant, and sufficient diffusion occurs to effectively digest the CSPGs. In humans, there might be a need for greater diffusion distances due to a deeper CSPG deposition zone, but whether or not chABC diffusion into injured human spinal cord will be a limitation remains to be determined.

While some sensory recovery was expected in the MTC, MTN, and MTCN groups due to sensory axonal sprouting, no improvement with the thermal pain threshold test was observed in any of the groups. This may be due to the spared fibers around the dorsal lateral fasciculus that help retain sensitivity in all groups independent of the lesion. In addition, the significant primary afferent sprouting in the treated animals was located predominantly in the dorsal white matter, with no fibers entering the lesion site in any of the groups. Our observation is consistent with other studies in which no improvement of noxious thermal sensation was observed despite robust primary afferent sprouting (5, 30).

We observed significant improvements in stride length in the MTCN group. Stride length is an important parameter of locomotor efficacy, affecting the speed of locomotion (31). The gains in other locomotor functions probably were obscured by our choice of the relatively mild hemisection injury model. Because microtube-mediated delivery resulted in enhanced serotonergic fiber sprouting relative to all other groups, with combinatorial delivery eliciting even more significant sprouting, it is possible that local serotonergic spinal circuits facilitated the observed locomotor improvements in stride length. This increase in sprouting is likely due to chABC-mediated digestion of CSPG-rich PNNs that surround synapses (32). PNNs may regulate neuronal plasticity (6), protect encapsulated neurons (33), and support ion homeostasis (34). Our observation is consistent with other reports that PNN digestion by chABC leads to increased plasticity and functional improvement due to reinnervation and sprouting (35, 36). Motor neurons and many interneurons are surrounded by PNNs, and the PNNs destabilized by chABC digestion would promote anatomic plasticity by increasing the density of newly grown processes in the adult CNS, which could lead functional plasticity. ChABC-induced plasticity, such as collateral sprouting (35) or aberrant sprouting (5), is a major mechanism of chABC treatment.

Possible negative effects are aberrant sprouting and neuropathic pain due to the aberrant plasticity (37) or autonomic dysreflexia due to increased plasticity (38). But no evidence of hyperalgesia was observed after chABC injection in to the spinal cord (7), and no increase in the connectivity of nociceptive neurons or the development of mechanical allodynia or thermal hyperalgesia was observed even after aberrant sensory fiber sprouting (5). Thus, it is perhaps important to balance detrimental sprouting and beneficial sprouting, and also to elucidate the molecular mechanism of chABC-mediated improvement of function and the contribution of plasticity. Interestingly, functional recovery was not observed until at least 6 weeks post-SCI, probably because axons retracted from the lesion site after injury, and outgrowth was not initiated until CSPG digestion rendered the substrate permissive to axon growth. Moreover, the effects of chABC may partially be due to anti-inflammatory and neuroprotective effects of the soluble disaccharidic end products of chABC-mediated digestion of CSPG (39, 40).

In conclusion, we have demonstrated that sustained local delivery of TS-chABC digests CSPGs after SCI without aggravating a secondary injury response. Combination therapy with chABC and NT-3 facilitated by our sustained delivery system was found to enhance axonal sprouting and functional recovery after SCI. This approach obviates the need for invasive, indwelling catheter/pump-mediated delivery of chABC, enables combination therapy with neurotrophic factors, and represents a promising approach to implementing chABC therapy after SCI.

Materials and Methods

See *SI Text* for further details.

Enzymatic Activity Assay. Trehalose at a concentration range of 20 mM–1 M in PBS was coincubated with 2 U/0.5 mL of chABC at 37 °C for 1, 2, 3, or 4 weeks. After incubation, 10 μL of decorin (5 μg) was added at 37 °C, and enzymatic digestion was allowed to proceed for 4 additional hours. The resulting product was analyzed by SDS-PAGE. Penicillinase (250 ng) was used as a negative control for enzyme activity. All experiments were performed with chABC from the same lot (Seikagaku). A DMMB assay was used to quantify sulfated CS-GAGs that remained intact after chABC-mediated digestion of decorin (15, 41). The absorbance of decorin digested by fresh chABC was considered to represent standard, 100% enzymatic activity. The percentage of sample absorbance relative to the standard was calculated, and a deactivation curve was plotted.

chABC Release Profiles From Lipid Microtubes. SDS-PAGE was used to examine any potential adverse effects of the lipid microtubes on chABC as a carrier for sustained release, such as loss of enzymatic activity. The DMMB assay was used to characterize the release profile of chABC from microtubes as described above. chABC/trehalose/microtubes and penicillinase/trehalose/microtubes were combined with SeaPlaque agarose (Cambrex), allowed to gel (18), placed in a 96-well plate, and incubated at 37 °C for up to 2 weeks. The collected supernatant was mixed with decorin, incubated at 37 °C, and analyzed by a DMMB assay as described above.

Analysis of Temperature-Dependent Conformation of chABC. The potential contribution of conformational changes to the thermal destabilization of chABC was investigated via CD studies with and without trehalose stabilization.

Topical Delivery of Agarose-Microtube-chABC Scaffolds After SCI and Retrograde Neuronal Tracer Injection Into the Sciatic Nerve. Adult male Sprague-Dawley rats (Charles River) received a dorsal-over-hemisection injury at the T-10 vertebral level. Sustained topical delivery of TS-chABC ($n = 8$; MTC) was achieved as reported previously (42) (Fig. S2). As controls, 10 mU of chABC in 10 μL of 1× PBS ($n = 6$; SC) or 1 M trehalose/1× PBS ($n = 6$; STC) were injected as "single-injection" conditions that have local but not sustained delivery. Then 55 ng of penicillinase (Sigma), the same amount as the total amount of delivered chABC, was delivered by single injection ($n = 6$; STP) or hydrogel-microtube scaffold ($n = 6$; MTP). Sham ($n = 4$), trehalose-loaded hydrogel scaffold conditions ($n = 6$; MT), and injury/NoT ($n = 6$) were used as well. After 2 weeks, the animals were euthanized, and the spinal cords were prepared for histological analysis. The surgical procedure for the 45-day study was the same as that for the 2-week study. Single-injection conditions were excluded, and 3 new conditions were added (see Table 1 for further details): 1% SeaPrep agarose mixed with 10 mU of ChABC ($n = 6$; GC), microtubes loaded with NT-3 ($n = 7$; MTN; 100 ng per rat), and combination microtubes loaded with chABC and NT-3 ($n = 8$; MTCN). Six weeks postinjury, 5 μL of 1% CTB (Sigma) was slowly injected into the nerve with a 34-gauge needle, and the animals were killed 3–4 days later and processed.

Behavioral Analysis. Locomotion and thermal pain sensitivity were assessed to determine functional improvement by investigators blinded with regard to animal groups using CatWalk (Noldus). Stride length, paw print pattern, and base support were chosen to examine behavioral as a function of time after injury for all experimental conditions. Thermal sensitivity was assessed by a dynamic plantar (Ugo Basile) described by Hargreaves, et al. (43), and each hind paw was tested 3 times every week and averaged.

Immunohistochemistry of Spinal Cords. The following primary antibodies were applied: antibody to the stub protein after chABC digestion (1:150, mouse IgM, clone 3-B-3; Seikagaku America), which recognizes unsaturated, C6-sulfated GAG stubs (17); CSPG (1:250, mouse IgM, clone CS-56; Sigma) to identify CSPGs; GFAP (1:600, polyclonal rabbit IgG; Chemicon) for astrocytes; WFA (5 μg/mL; Sigma) for perineuronal nets; and anti-CTB (1:600; Abcam) and serotonin (1:150, 5-HT, monoclonal mouse IgG1; Abcam) for serotonergic neurons. The following secondary antibodies were used: goat anti-rabbit IgG (H+L) Alexa Fluor 488 (1:200; Invitrogen) for GFAP, goat anti-mouse IgM Alexa Fluor 594 (1:200) for 3B3 and CS-56, and streptavidin Alexa Fluor 488 for WFA.

Quantitative Analysis of CSPG Digestion, Astrocyte Response, and Axonal Sprouting. At least 4 animals were chosen from each animal group, 4 sections were chosen from each animal, and 5 images were captured. The GFAP-IR images were analyzed with a custom-built image analysis program (MATLAB; Mathworks) (18). For 3B3-IR, CS-56–IR, and serotonin (5-HT) immunofluorescence, relative intensity was measured with ImagePro software (MediaCybernetics) and averaged. A montage of each tissue section stained for CTB-labeled fibers was obtained at 10× magnification using Neurolucida software (MicroBrightField Bioscience). The percentage of CTB fibers that stopped within the defined regions was determined after accounting for background intensity.

Statistical Analysis. Minitab software was used to determine the statistical differences between experimental conditions (ANOVA). A P value $< .05$ was considered to represent a statistically significant difference.

ACKNOWLEDGMENTS. We thank Professor Andreas Bommarius for assistance with the CD analysis; Vivek Mukhatyar, Lohitash Karumbaiah, and Samuel Beckerman for technical discussions; and Janki Patel and Arun Duraiswamy for their assistance with behavioral studies. This work was supported by National Institutes of Health Grant R01 NS043486 (to R.V.B.).

1. Schwab ME, Bartholdi D (1996) Degeneration and regeneration of axons in the lesioned spinal cord. *Physiol Rev* 76:319–370.
2. McKeon RJ, Schreiber RC, Rudge JS, Silver J (1991) Reduction of neurite outgrowth in a model of glial scarring following CNS injury is correlated with the expression of inhibitory molecules on reactive astrocytes. *J Neurosci* 11:3398–3411.
3. Fawcett JW, Asher RA (1999) The glial scar and central nervous system repair. *Brain Res Bull* 49:377–391.
4. Bradbury EJ, et al. (2002) Chondroitinase ABC promotes functional recovery after spinal cord injury. *Nature* 416:636–640.
5. Barritt AW, et al. (2006) Chondoroitinase ABC promotes sprouting of intact and injured spinal systems after spinal cord injury. *J Neurosci* 26:10856–10867.
6. Pizzorusso T, et al. (2002) Reactivation of ocular dominance plasticity in the adult visual cortex. *Science* 298:1248–1251.
7. Pizzorusso T, et al. (2006) Structural and functional recovery from early monocular deprivation in adult rats. *Proc Natl Acad Sci USA* 103:8517–8522.
8. Tester NJ, Plaas AH, Howland DR (2007) Effect of body temperature on chondroitinase ABC's ability to cleave chondoroitin sulfate glycosaminoglycans. *J Neurosci Res* 85:1110–1118.
9. Jones LL, Margolis RU, Tuszynski MH (2003) The chondroitin sulfate proteoglycans neuroncan, brevican, phosphacan, and versicam are differentially regulated following spinal cord injury. *Exp Neurol* 182:399–411.
10. Chau CH, et al. (2004) Chondroitinase ABC enhances axonal regrowth through Schwann cell–seeded guidance channels after spinal cord injury. *FASEB J* 18:195–196.
11. Caggiano AO, Zimber MP, Ganguly A, Blight AR, Gruskin EA (2005) Chondroitinase ABCI improves locomotion and bladder function following contusion injury of the rat spinal cord. *J Neurotrauma* 22:226–239.
12. Houle JD, et al. (2006) Combining an autologous peripheral nervous system "bridge" and matrix modification by chondroitinase allows robust, functional regeneration beyond a hemisection lesion of the adult rat spinal cord. *J Neurosci* 26:7405–7415.
13. Haung WC, et al. (2006) Chondroitinase ABC promotes axonal regrowth and behavior recovery in spinal cord injury. *Biochem Biophys Res Commun* 349:963–968.
14. Greenfield NJ (1999) Applications of circular dichroism in protein and peptide analysis. *Trends Anal Chem* 18:236–244.
15. Melrose J, Ghosh P (1988) The quantitative discrimination of corneal type I, but not skeletal type II, keratan sulfate in glycosaminoglycan mixtures by using a combination of dimethylmethylene blue and endo-beta-D-galactosidase digestion. *Anal Biochem* 170:293–300.
16. de Jong JG, Wevers RA, Laarakkers C, Poorthuis BJ (1989) Dimethylmethylene blue–based spectrophotometry of glycosaminoglycans in untreated urine: A rapid screening procedure for mucopolysaccharidoses. *Clin Chem* 35:1472–1477.
17. Baker JR, Christner JE, Ekborg SL (1991) An unsulphated region of the rat chondrosarcoma chondroitin sulphate chain and its binding to monoclonal antibody 3B3. *Biochem J* 273:237–239.
18. Jain A, Kim YT, McKeon RJ, Bellamkonda RV (2006) In situ gelling hydrogels for conformal repair of spinal cord effects, and local delivery of BDNF after spinal cord injury. *Biomaterials* 27:497–504.
19. Hédoux A, et al. (2009) Thermostabilization mechanism of bovine serum albumin by trehalose. *J Phys Chem B* 113:6119–6126.
20. Crowe LM, Mouradian R, Crowe JH, Jackson SA, Womersley C (1984) Effects of carbohydrates on membrane stability at low water activities. *Biochim Biophys Acta* 769:141–150.
21. Timasheff SN (2002) Protein–solvent preferential interactions, protein hydration, and the modulation of biochemical reactions by solvent components. *Proc Natl Acad Sci USA* 99:9721–9726.
22. Green JL, Angell CA (1989) Phase relations and vitrification in saccharide-water solutions and the trehalose anomaly. *J Phys Chem* 93:2880–2882.
23. Branca C, Magazu S, Maisano G, Migliardo P (1999) Anomalous cryoprotective effectiveness of trehalose: Raman scattering evidence. *J Chem Phys* 111:281–287.
24. Kita Y, Arakawa T, Lin TY, Timasheff SN (1994) Contribution of the surface free energy perturbation to protein–solvent interactions. *Biochemistry* 33:15178–15189.
25. Kaushik JK, Bhat R (2003) Why is trehalose an exceptional protein stabilizer? *J Biol Chem* 278:26458–26465.
26. Iseda T, et al. (2008) Single, high-dose intraspinal injection of chondroitinase reduces glycosaminoglycans in injured spinal cord and promotes corticospinal axonal regrowth after hemisection but not contusion. *J Neurotrauma* 25:334–349.
27. Meilander NJ, Yu X, Ziats NP, Bellamkonda RV (2001) Lipid-based microtubular drug delivery vehicles. *J Control Release* 71:141–152.
28. Meilander NJ, Pasumarthy MK, Kowalczyk TH, Cooper MJ, Bellamkonda RV (2003) Sustained release of plasmid DNA using lipid microtubules and agarose hydrogel. *J Control Release* 88:321–331.
29. Yu X, Bellamkonda RV (2003) Tissue-engineered scaffolds are effective alternatives to autografts for bridging peripheral nerve gaps. *Tissue Eng* 9:421–430.
30. Cafferty WB, Yang SH, Duffy PJ, Li S, Strittmatter SM (2007) Functional axonal regeneration through astrocytic scar genetically modified to digest chondroitin sulfate proteoglycans. *J Neurosci* 27:2176–2185.
31. Hamers FP, Lankhorst AJ, van Laar TJ, Veldhuis WB, Gispen WH (2001) Automated quantitative gait analysis during overground locomotion in the rat: Its application to spinal cord contusion and transection injuries. *J Neurotrauma* 18:187–201.
32. Vitellaro-Zuccarello L, De Biasi S, Spreafico R (1998) One hundred years of Golgi's "perineuronal net": History of a denied structure. *Ital J Neurol Sci* 19:249–253.
33. Brückner G, et al. (1999) Cortical areas abundant in extracellular matrix chondroitin sulphate proteoglycans are less affected by cytoskeletal changes in Alzheimer's disease. *Neuroscience* 92:791–805.
34. Brückner G, et al. (1993) Perineuronal nets provide a polyanionic, glia-associated form of microenvironment around certain neurons in many parts of the rat brain. *Glia* 8:183–200.
35. Massey JM, et al. (2006) Chondroitinase ABC digestion of the perineuronal net promotes functional collateral sprouting in the cuneate nucleus after cervical spinal cord injury. *J Neurosci* 26:4406–4414.
36. Galtrey CM, Asher RA, Nothias F, Fawcett JW (2007) Promoting plasticity in the spinal cord with chondroitinase improves functional recovery after peripheral nerve repair. *Brain* 130:926–939.
37. Woolf CJ, Salter MW (2000) Neuronal plasticity: Increasing the gain in pain. *Science* 288:1765–1769.
38. Weaver LC, Marsh DR, Gris D, Brown A, Dekaban GA (2006) Autonomic dysreflexia after spinal cord injury: Central mechanisms and strategies for prevention. *Prog Brain Res* 152:245–263.
39. Rolls A, et al. (2006) A sulfated disaccharide derived from chondroitin sulfate proteoglycan protects against inflammation-associated neurodegeneration. *FASEB J* 20:547–549.
40. Rolls A, et al. (2004) A disaccharide derived from chondroitin sulphate proteoglycan promotes central nervous system repair in rats and mice. *Eur J Neurosci* 20:1973–1983.
41. Gilbert RJ, et al. (2005) CS-4,6 is differentially upregulated in glial scar and is a potent inhibitor of neurite extension. *Mol Cell Neurosci* 29:545–558.
42. Chvatal SA, Kim YT, Bratt-Leal AM, Lee H, Bellamkonda RV (2008) Spatial distribution and acute anti-inflammatory effects of methylprednisolone after sustained local delivery to the contused spinal cord. *Biomaterials* 29:1967–1975.
43. Hargreaves K, Dubner R, Brown F, Flores C, Joris J (1988) A new and sensitive method for measuring thermal nociception in cutaneous hyperalesia. *Pain* 32:77–88.